Water Air Soil Pollut (2022) 233: 118
https://doi.org/10.1007/s11270-022-05600-1

Design and Application of Homogeneous-structured TiO_2/Activated Carbon Nanocomposite for Adsorption–Photocatalytic Degradation of MO

Osi Arutanti · Anggun Lila Sari · Christina Wahyu Kartikowati · Ajeng Arum Sari · Aditya Farhan Arif

Received: 16 November 2021 / Accepted: 23 March 2022 / Published online: 30 March 2022

Abstract The sol–gel method successfully prepared homogeneous-structured TiO_2/activated carbon (TiO2/AC). This study highlights the effect of post-annealing temperature on the properties and photocatalytic activity of composite TiO_2/AC to remove methyl orange (MO). The prepared photocatalysts were characterized by X-ray diffraction (XRD), scanning electron microscope (SEM), transmission electron microscope (TEM), Brunauer–Emmett–Teller measurement (BET), and thermogravimetric (TGA). The results confirmed that all prepared photocatalysts were TiO_2 anatase. The removal of MO was obtained through a synergistic effect of adsorption and photocatalysis. TiO_2/AC-400 was the optimum photocatalyst to decompose MO up to 80% after 90 min under simulated UV irradiation. The remaining 1% AC after the annealing process at 500 °C had proved to be capable of decomposing MO mainly due to its serving as an electron trap. The potential photocatalyst formation and photocatalysis mechanism for TiO_2/AC nanocomposite to support phenomena were proposed. The finding in this study provided important implications for further research on the preparation of composite TiO_2 and carbon-based co-catalyst to enhance the adsorption–photocatalytic activity.

Keywords Electron-trap · Nanoparticles · Nanocomposite · Photocatalyst

O. Arutanti (✉) · A. L. Sari
Research Center for Advanced Chemistry, National Research and Innovation Agency, Serpong, Indonesia
e-mail: osiarutanti@yahoo.com

C. W. Kartikowati
Department of Chemical Engineering, Universitas Brawijaya, Malang, Indonesia

A. A. Sari
Research Unit for Clean Technology, National Research and Innovation Agency, Bandung, Indonesia

A. F. Arif
Indonesia Mining and Mineral Research Institute, Mining Industry Indonesia (MIND ID), Jakarta, Indonesia

1 Introduction

The residual of organic dyes, such as azo dye, is one of the major contaminants of industrial wastewater due to their toxic nature. Azo dyes such as methyl orange, rhodamine B, and methylene blue are the largest group and the most frequently used as colorants due to cost-effectiveness and ease of use compared to natural dyes (Benkhaya et al., 2020). However, most organic dyes are delicate. Their high stability under sunlight irradiation, temperature, and biodegradation makes it unbreakable naturally quickly (Lellis et al., 2019). Therefore, the presence of this pollutant affected the natural water ecosystem and human health (Lellis et al., 2019). Because the increased demand for textile products is a proportional increase in the use of organic dyes, it is crucial to develop

effective, efficient, end environmentally friendly technology to overcome the effect problems.

Among the technology, photocatalysis is one of the promising methods to decompose organic dyes. Titanium dioxide (TiO_2)-based photocatalytic as the common photocatalyst for water treatment technology is rapidly growing due to its environmentally friendly characteristic, resistance to photo-corrosion, low cost, long-term stability, and oxidation power (Qi et al., 2017). Unfortunately, low visible-light absorption due to the bandgap energy value (3.2 eV) and photogenerated charge ability, which causes a short recombination process, is the significant drawback of TiO_2 (Qi et al., 2017). In recent years, heterogeneous catalysis has found great application. Creating the binary metal oxide system (ZnO, WO_3, SiO_2, etc.), metal- (Pt, Ag, Au, etc.) and non-metal-doped (N, S, etc.) photocatalyst and carbon-supported photocatalyst material have been proposed as the solution technique to overcome the disadvantages of TiO_2-based photocatalyst (Arutanti et al., 2014a; Daghrir et al., 2013). Among those, the combination of TiO_2 photocatalyst and carbonaceous material is one solution to enhance photocatalytic efficiency through three mechanisms: enhanced absorption of visible light and facile charge separation and transportation higher adsorption of pollutants, especially for the high-concentration pollutant degradation (Anthonysamy et al., 2018; Krýsa et al., 2020; Lim et al., 2011).

The use of activated carbon (AC) has drawn significant attention application compared to various types of carbonaceous material supports such as nanotubes (CNTs), carbon quantum dots (Cdot), and graphene (Gr) owing to their properties such as stability, economically cost, and the specific surface area (Andriantsiferana et al., 2015; Anthonysamy et al., 2018; Krýsa et al., 2020; Lee & Jo, 2012; Lim et al., 2011; Ouzzine et al., 2014; Peñas-Garzón et al., 2019). It has been reported that supported activated carbon on the TiO_2 to decompose organic pollutants has a synergistic effect based on adsorption capacity and the photocatalytic (Krýsa et al., 2020; Peñas-Garzón et al., 2019). High adsorption capability was due to high specific surface area and carbon-based material's chemical surface (Syed et al., 2019). Furthermore, the physicochemical properties of carbon-based material also influence the TiO_2 photocatalytic activity (Syed et al., 2019). Several reported papers suggested the typical micro- and mesoporous framework to enhance the photodegradation, i.e., Garzon et al. (Peñas-Garzón et al., 2019) proposed the composite of TiO_2/AC by the solvothermal method. They succeed in preparing nano-sized spherical particles (Peñas-Garzón et al., 2019). However, the result showed that the photocatalytic activity of bare TiO_2 was higher than that of TiO_2/AC. Krysa et al. reported the synthesis of composite TiO_2/C for air pollutant removal (Krýsa et al., 2020). Unfortunately, they used TiO_2 P25 commercial, which has been known to have excellent photocatalytic activity under UV light. Lu et al. succeed in removing MO by using TiO_2/biochar as a catalyst (Lu et al., 2019).

Various methods of synthesis TiO_2/AC composite have been reported (Horikoshi et al., 2013; Soleymani Naeini et al., 2019; Subramani et al., 2007; Syed et al., 2019; Yin et al., 2017; Zhang & Lei, 2008). The synthesis method will influence the characteristics and morphology of the photocatalyst material. The sol–gel method is one of the standard methods for synthesizing nanoparticles due to their advantages, such as a wide variety of morphology and low-cost production cost. The sol–gel process generally consists of hydrolysis and condensation of metal alkoxides in aqueous media (Parashar et al., 2020). The presence of water triggered the hydrolysis process followed by the nucleation and growth process rapidly to form tridimensional oxide particles (Esposito 2019). Since this method produced metal oxide with low crystallinity, the heat treatment process is required.

Even though the preparation of composite TiO_2 and activated carbon by the sol–gel method has been widely published, some phenomena explanations are still lacking. For example, they mentioned whether the presence of activated carbon could enhance photocatalytic activity. However, unfortunately, the actual effect of AC on the adsorption and photocatalytic activity in their work did not explain comprehensively.

The current project embarks on the homogeneous-structured TiO_2/activated carbon nanocomposite design via the sol–gel method. This present work addresses the preparation of pure TiO_2 and TiO_2/AC nanocomposites for different post-annealing treatment temperatures ranging from 200 to 500 °C and their application to remove methyl orange (MO). Specifically, the presence of a small amount of AC to improve photocatalytic activity was examined.

Furthermore, this research article includes the proposed TiO_2/AC composite formation mechanism and adsorption–photocatalytic activity to enlighten all phenomena.

2 Experimental Setup

2.1 Synthesis of TiO_2/AC

Composite of TiO_2/AC was prepared by the sol–gel method. Titanium (IV) ethoxide ($Ti(OEt)_4$, Sigma Aldrich, USA) and commercial activated carbon (AC, Sigma-Aldrich, USA) were used as TiO_2 and carbon sources, respectively. Ethanol (Merck, USA) was used as precursors. In the preparation of TiO_2 using the sol–gel method, 5.24 mL of titanium (IV) ethoxide was dissolved in 20 ml of ethanol (ETOH, analytical grade, Sigma-Aldrich) and stirred for 15 min. Next, 10 mL of distilled water was dropped into the solution, stirred for 60 min, and dried for 12 h at 100 °C. The resulted sample was labeled as TiO_2-100. As a reference, another TiO_2 sample annealed at 500 °C was prepared and labeled as TiO_2-500.

The same synthesis protocol was used to prepare TiO_2/AC composites, except that AC nanoparticle powder ($D_p = 50$ nm) was added into the precursor with a TiO_2/AC ratio of 1:3 and stirred for 10 min before the addition of distilled water. The prepared particles were then annealed under various temperatures, *i.e.,* 200, 300, 400, and 500 °C for 120 min, and the sample was, respectively, labeled as TiO_2/AC-200, TiO_2/AC-300, TiO_2/AC-400, and TiO_2/AC-500. The preliminary research to obtain the optimum TiO_2/AC ratio has been proposed in the previous work (Kartikowati et al., 2021).

2.2 Characterization

X-ray diffraction (XRD, PANalytical, Japan; using CuKα radiation and 2θ scanning range of 20–80°) has been used to examine the phase and crystal size of the prepared particles. Scanning electron microscope (SEM, JEOL JIB 4610F) and transmission electron microscope (TEM, Tecnai G2 20 S-TWIN) have been used to depict the particle morphology of the prepared particle. The specific surface area was analyzed using the Brunauer–Emmett – Teller measurement (BET; BELSORP 28SA, Bel, Japan, nitrogen adsorption isotherms at 77.15 K). Fourier transform infrared spectroscopy was used to determine the functional groups of the TiO_2 framework. The remainder of activated carbon was analyzed by thermogravimetric analysis (TGA).

2.3 Photocatalysis Performance

Methyl orange (MO, Merck, USA) was analyzed as a waste organic pollutant model over the prepared photocatalysts under UVC light. In a typical experiment, 800 mg L^{-1} of the prepared catalyst has been adjusted to decompose four ppm MO. Four milliliters of the mixed solution was sampled for several minutes. Before analysis, collected samples after photocatalysis were centrifuged at 10,000 rpm for 5 min. The MO concentration in the sample was measured using a UV – Vis spectrophotometer (UV3150; Shimadzu Corp., Japan) in the wavelength range of 200–700 nm. The process was 60 min under dark conditions and 90 min under UV-light illumination. Degradation efficiency (%) of MO is calculated by Eq. (1) as follows (Arutanti et al., 2020):

$$\text{Degradation efficiency}(\%) = \left(\frac{C_0 - C_t}{C_0}\right) x100 \quad (1)$$

where C_0 is the concentration of MO, and Ct is the remaining concentration of MO after 90 min.

3 Results and Discussion

3.1 Physicochemical Properties

As shown in Fig. 1, XRD of all the prepared composite particles shows the characteristic peaks of the TiO_2 anatase phase referred to the JCPDS number 21–1272. It is important to remark that no other rutile or brookite phases were observed in any of the annealed TiO_2/AC composite particles, showing that the current synthesis route was temperature-controlled. To observe the effect of annealing temperature, the average crystal (Dc) size was calculated based on Scherrer's equation (Kibasomba et al., 2018) applied to the intense peak of anatase (101). Dc of pure TiO_2 at 100 °C was 17.47 nm. The different annealing temperature processes implied the more substantial peak of anatase (101), indicating

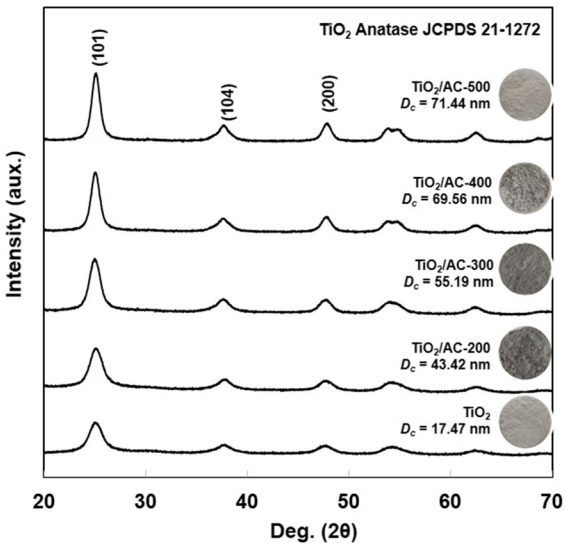

Fig. 1 XRD patterns of the prepared TiO_2/AC under various post-annealing temperature treatments

the enhancement of *Dc*. By increasing the annealing temperature from 200, 300, 400, and 500 °C, the *Dc* value increased from 43.42 nm to 55.19, 69.56, and 71.44 nm, respectively. Annealed pure TiO_2 at 500 °C (TiO_2-500) showed the most significant *Dc* at 109 nm. Hence, it can be inferred that TiO_2/AC with a higher Dc may effectively reveal the degradation efficiency of MO (Arutanti et al., 2014b). Insert photograph images further supported the presence of activated carbon. Annealing temperature under the air atmosphere influenced the color of the prepared composite TiO_2/AC. Low annealing temperatures (200 and 300 °C) produced the darker (grey) particles, while, at the higher temperature, AC started to decompose, resulting in the TiO_2/AC composite with the lighter color. Based on the photocatalyst color, AC significantly decomposed over 400 °C. Even though the TiO_2-500 and TiO_2/AC-500 °C had similar colors, they have different crystallite sizes, indicating that the presence of AC inhibited the crystallinity growth.

SEM images revealed the prepared particles as shown in Fig. 2. The use of pure TiO_2 with the post-annealing treatment of 500 °C is proposed in Fig. 2a. The prepared TiO_2/AC composite was spherical (Fig. 2b-2d) with a mean diameter (D_p) of approximately in the range of 100–200 nm. The particle diameter increased with the increasing annealing temperature. As a result, the sintered and bigger particles were found. The insert figures showed that the prepared TiO_2/AC had a rough surface composed of primary TiO_2 NPs. It can be noted that AC could not be observed in the SEM images. Therefore, detailed microstructure information of TiO_2/AC-400 is presented by TEM and HRTEM images in Fig. 2(f)–2(g). The black color in Fig. 2(f) depicted the trapped AC covered by TiO_2 nanoparticles. The HRTEM image in Fig. 2(g) exhibits the crystalline structure of TiO_2 anatase with the lattice fringe of 3.45 nm (Arutanti et al., 2014a). A detailed mechanism of TiO_2/AC formation will propose in the next part.

EDS elemental mapping to confirm elements distribution on the prepared TiO_2-100, TiO_2/AC-300, TiO_2/AC-400, and TiO_2/AC-500 composite is presented in Fig. 3. Red, turquoise, and green correspond to Ti, O, and C elements, respectively. C element was not found in TiO_2-500 (Fig. 3(a)), indicating that the synthesis route produced pure TiO_2 without C contamination. The presence of the C element can be confirmed in the samples added with AC during the preparation (Fig. 3(b)–3(d)). In general, Ti, O, and C distribution was homogeneous, confirming that all elements were well dispersed on the prepared TiO_2/AC composite particles. Here, annealing temperature reduced the amount of AC, indicated by the decreasing intensity of the C spectrum with the increasing annealing temperature. Over 400 °C (Fig. 3(c)-(d)), the green color was still detected, indicating the presence of C, even though the particles were white. It was assumed that a small number of AC were still trapped on the TiO_2 primary particles.

Nitrogen adsorption–desorption isotherm and BJH analysis revealed quantifying the specific surface area (S_{BET}), pore size (D_{pore}), and pore volume (V_{pore}) of them all prepared photocatalyst (Fig. 4). All the isotherms correspond to Type IV with a remarkably vertical hysteresis conforming to the H4 hysteresis loop in IUPAC standard, attributed to the combination of mesoporous and microporous structure. It was assumed that the mesoporous structure in the isotherm was due to the aggregation of TiO_2, as confirmed by the TEM results in Fig. 2, while the observed microporous structure was further clarified from the evaluation S_{BET} and V_{pore}.

TiO_2-500 was measured as a reference of a pure TiO_2 sample to be compared with the composites. Based on Brunauer–Emmett–Teller (BET) calculation, the specific surface area of TiO_2-500 was 57.28

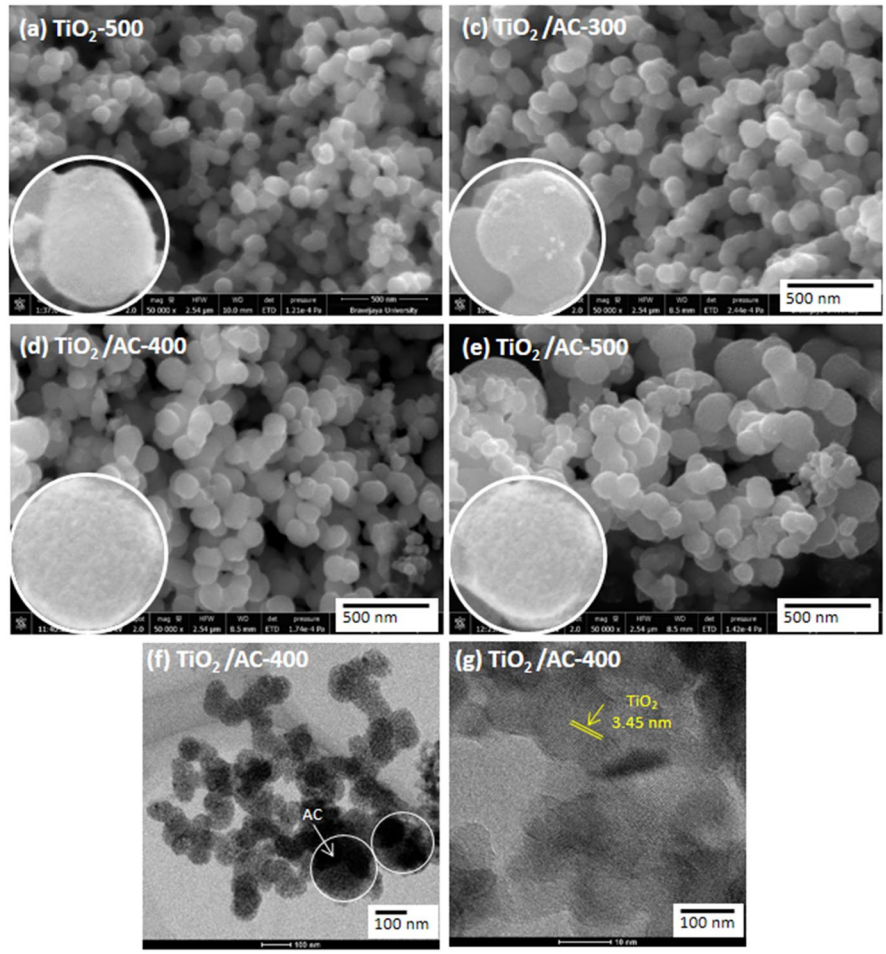

Fig. 2 SEM images of the prepared photocatalyst (**a**) without additional AC, (**d-d**) under various post-annealing temperature treatments and (**f-g**) TEM and HRTEM images of TiO_2/AC-400

m^2g^{-1}. The value of S_{BET} of TiO_2/AC-200, TiO_2/AC-300, TiO_2/AC-400, and TiO_2/AC-500 was 418, 294, 138, and 109 m^2g^{-1}, and the V_{pore} was 0.45, 0.33, 0.21, and 0.26 cm^{-1} g^{-1}, respectively. It is worth noting that S_{BET} of TiO_2/AC-500 was higher than that of TiO_2-500 despite having a larger particle size and being annealed at the same temperature. These results suggested that the remaining AC in TiO_2/AC-500 contained micropores, significantly improving the specific surface area. TiO_2/AC-200 exhibited the highest $S_{BET,}$ which confirmed the EDS result that this sample had the highest AC amount. The decrease of S_{BET} and V_{pore} was attributed to the increasing decomposition ratio of AC with the temperature. Based on the BJH analysis result, the average pore size of the prepared particles was in the range of 4–10 nm.

The FTIR spectra of the prepared catalysts are shown in Fig. 5. The spectra showed a similar peak in surface chemical functional groups, where the stretching absorption band in the 500–1000 cm^{-1} range corresponds to the skeletal O-Ti. A peek at about 1100 cm^{-1} referred to the presence of Ti–O–C. This peak cannot be found at TiO_2-500. Other clear signals were attributed to the C=O and O–H groups at 1671 cm^{-1} and 3500 cm^{-1}, respectively. This analysis result also confirmed the different compositions of AC between TiO_2-500 and TiO_2/AC-500. It was clearly verified that AC nanoparticles remained on the TiO_2/AC-500 detected by the bond of Ti–O–C at around 1100 nm.

The detailed mechanism of the composite TiO_2/AC formation is proposed in Fig. 6. In general, the process consisted of four steps: simultaneous hydrolysis and heterogeneous nucleation, homogeneous nucleation, and grain growth to produce primary particles of TiO_2. Finally, the primary particles of TiO_2

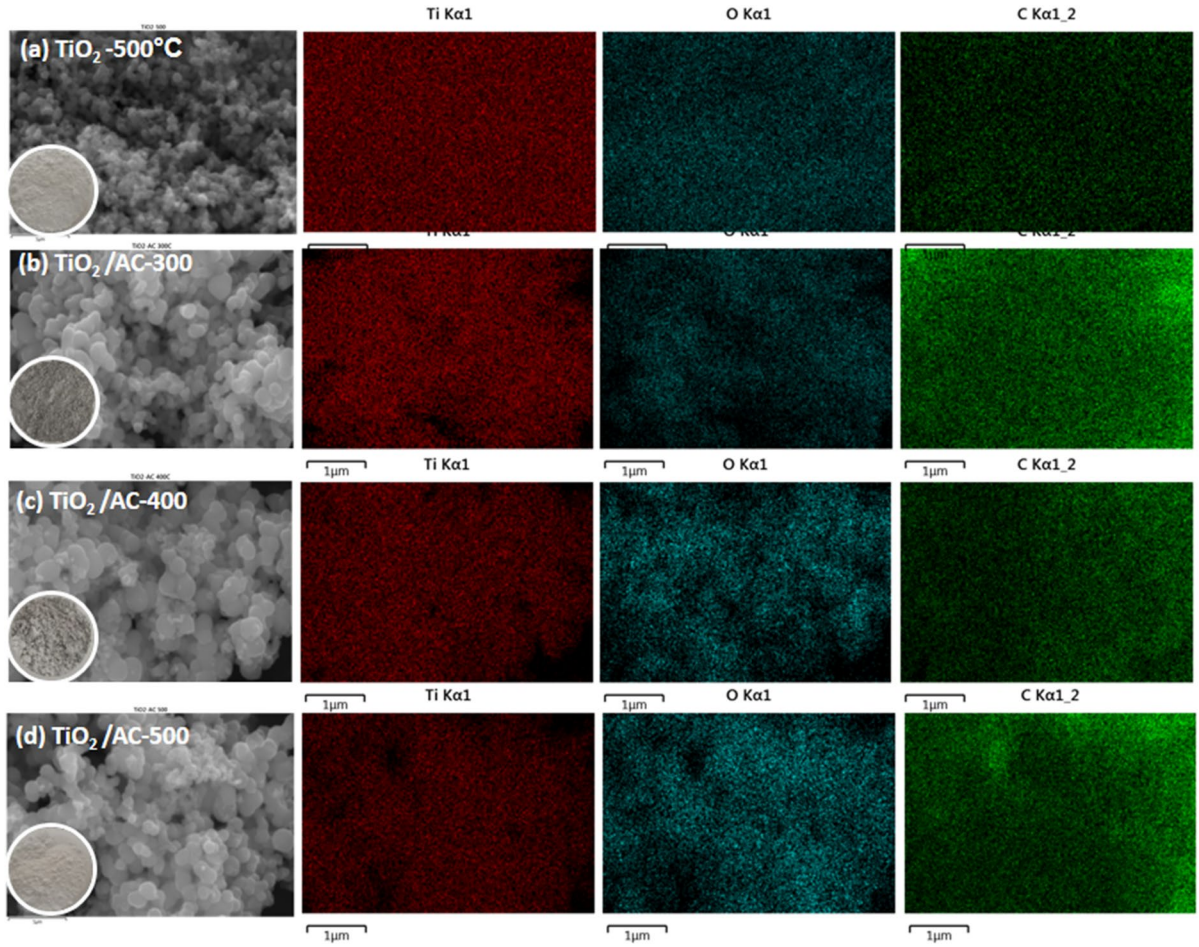

Fig. 3 Elemental mapping of (a) TiO_2 annealed at 500 °C and TiO_2/AC composite after annealing at (b) 300, (c) 400, and (d) 500 °C, and their respective SEM images

aggregated and formed secondary, bigger particles of TiO_2.

When water droplets reacted with $Ti(OEt)_4$ and EtOH solution, Ti-molecular clusters were generated through the hydrolysis–condensation reaction. The hydrolysis involved the scission of ethoxide ligands prior to the substitution with hydrogen. This step likely promoted attractive force between positively charged, unpaired Ti with the negatively charged hydroxyl group of AC, which induced heterogeneous nucleation of $\equiv T-OH$ onto the AC surface. As the hydrolysis and condensation proceeded, Ti-molecular clusters were formed. Homogenous nucleation of these clusters was followed by the formation of sol Ti-particles, namely primary particles. The primary particles were indicated by white arrows and white circles in the insert TEM images in Fig. 6. The heterogeneous nucleation allowed good mixing of carbon and titanium constituents in the composite structure. This characteristic differentiates the results of this synthesis protocol from those of previous works (Kartikowati et al., 2021).

Theoretically, the size of the primary particles should depend on the hydrolysis–condensation and chemistry of the solution. The size of primary particles in this work was approximately 10 nm. The collision process between the primary particles created the porous structure, as confirmed in TEM images in Fig. 2(e–f) and BJH analysis results. At this point, the final morphology of the particles was strongly affected by the amount of water. At the same time, the amount of ethanol affected

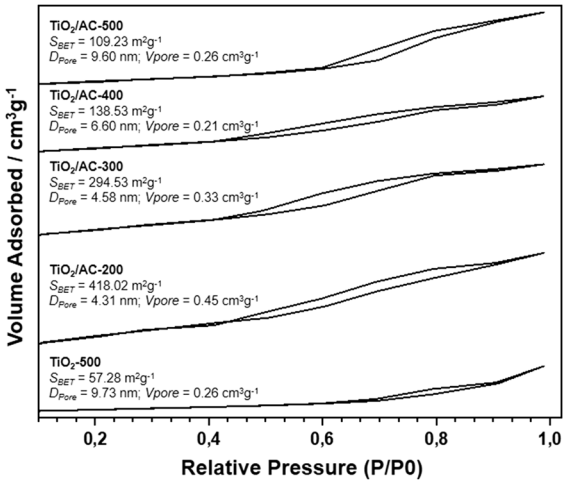

Fig. 4 N_2 adsorption–desorption isotherm of the prepared composite TiO_2/AC

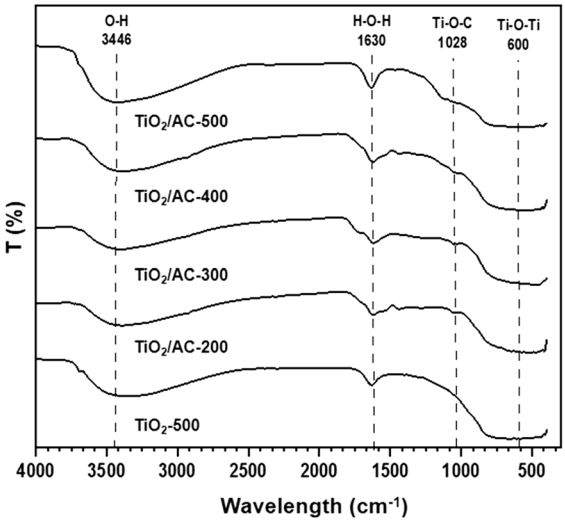

Fig. 5 FTIR spectra of the prepared photocatalyst TiO_2/AC

the speed of the hydrolysis reaction. Interaction between the colloidal particles created the porous structure and bigger particles, namely secondary particles, depicted by yellow arrows and circles in Fig. 6. During the sol–gel process, the sol particles can further associate with each other via collision within a certain period of aging to produce bigger isolate gel composite particles. After drying at 100 °C, a nanocomposite of TiO_2/AC with a bigger size and irregular shape was produced. The result was confirmed by the SEM image of the TiO_2-100 in Fig. 2(a).

In the post-synthesis annealing process, composite TiO_2/AC morphology evolution occurred. The annealing process triggered the grain growth and the sintering of the primary particles, resulting in the large crystallite size confirmed by XRD results in Fig. 1. Moreover, the sintering between primary particles resulted in the secondary necking of particle phenomenon (red arrows). Accordingly, it was easy to find the necking secondary particles on the annealed composite TiO_2/AC (Fig. 2(c)-2(e)), likely because of the sintering of TiO_2 nanocrystalline constituent, which starts at 200 °C (Hahn et al., 1990). This phenomenon is almost similar to another work (Ho et al., 2017). Interestingly, in the present work, the diameter of the secondary particles could still be controlled at around 100 nm and hence nanocomposite. The TEM images clearly show that the spherical TiO_2/AC composite was composed of aggregated, homogeneously distributed, the primary TiO_2 NPs and AC NPs.

During the annealing, the carbon constituent in the composite was decomposed. The degree of decomposition was depended upon the annealing temperature, resulting in the nanocomposites with different levels of color gradation as previously discussed. The heterogeneous nucleation in the early step composite formation even after 500 ℃, the homogeneous distribution of TiO_2 and AC triggering the remained of AC within the composite structure. The phenomenon was proved by the thermogravimetry (TG) analysis curves in Fig. 7. The weight loss comparison of the prepared photocatalyst, i.e., TiO_2/AC-200, TiO_2/AC-400, and TiO_2/AC-500, was analyzed. The first weight loss of around 250 °C was due to synthesizing remaining water and organic residues. Over 500 °C, the weight loss corresponds to the decomposition of surface oxygen groups. The difference of eight losses from the three samples was evidenced in the presence of AC. Based on the TG analysis results, the calculated remainder of AC from TiO_2/AC-200, TiO_2/AC-400, and TiO_2/AC-500 was 11, 2, and 1 wt% of AC, respectively. The mass loss in sample TiO_2/AC-500 confirmed that the post-annealing process at 500 °C leaves 1 wt% AC trapped in the composite particles. EDS also approved the result.

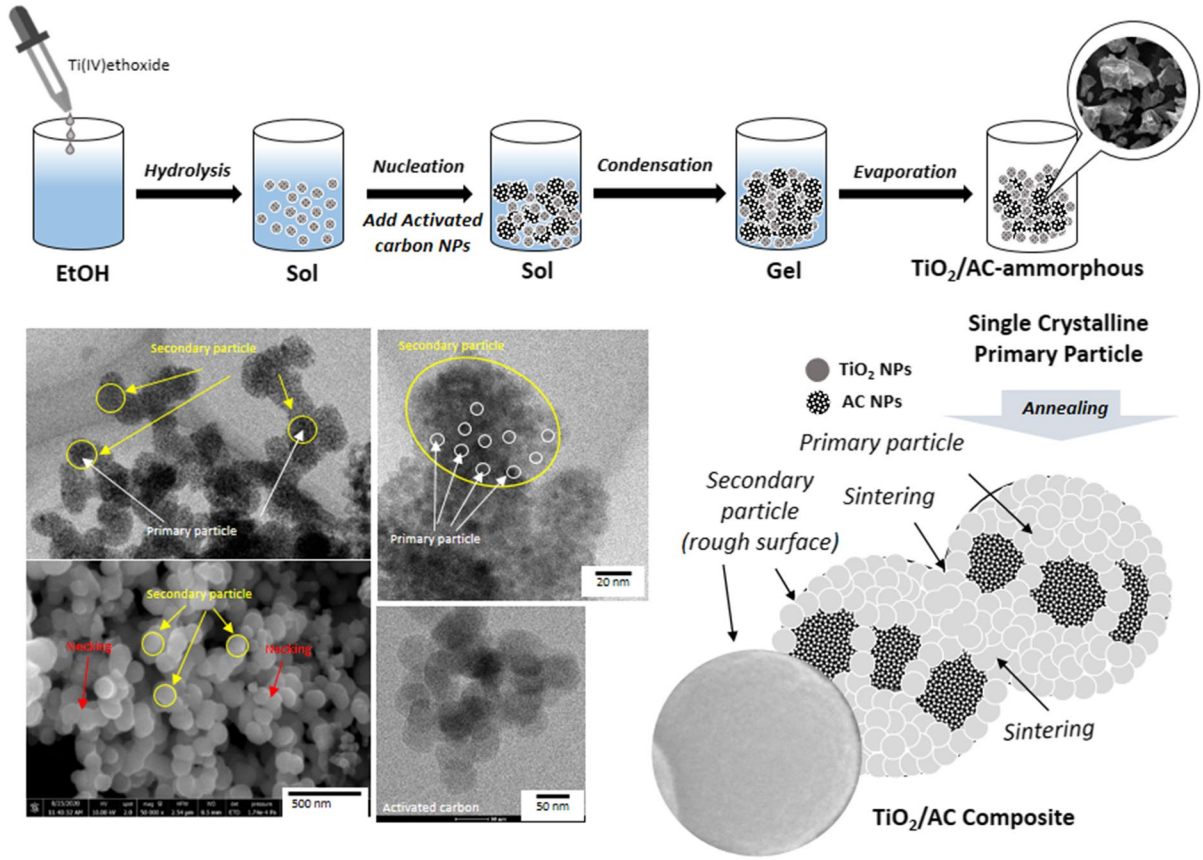

Fig. 6 Proposed mechanism of the composite TiO_2/AC formation

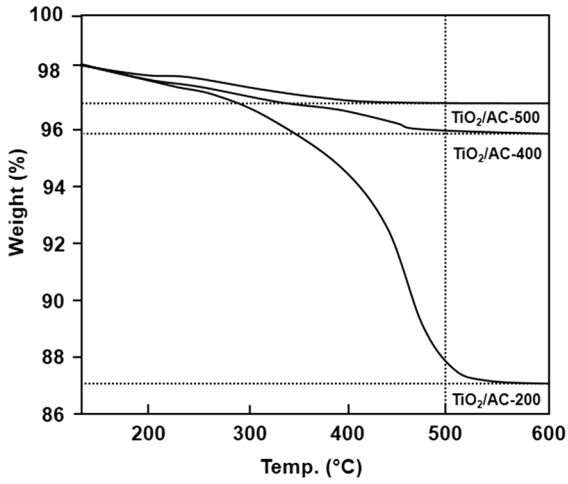

Fig. 7 TG spectra of the prepared photocatalyst TiO_2/AC under different annealing temperatures

3.2 Photodegradation by TiO_2/AC Composite Material

Photodegradation of MO using the prepared TiO_2/AC catalyst under UV irradiation is shown in Fig. 8. As a reference, pure TiO_2-500 was used. The result showed that TiO_2-500 had the lowest adsorption and photodegradation activity. Under dark conditions for 60 min, the degradation of MO was almost stable. However, after photocatalysis for 90 min, 60% of MO remained present. As mentioned in the previous section, the presence of activated carbon will enhance the specific surface area of the catalyst. The degradation may also contribute to the high dye absorbance. Thus, the composite of TiO_2/AC had a higher adsorption activity than that shown by pure TiO_2. During the dark period, 100% of MO was adsorbed by TiO_2/AC-200 and TiO_2/AC-300 owing to the high specific surface area. Excess AC in the prepared catalyst

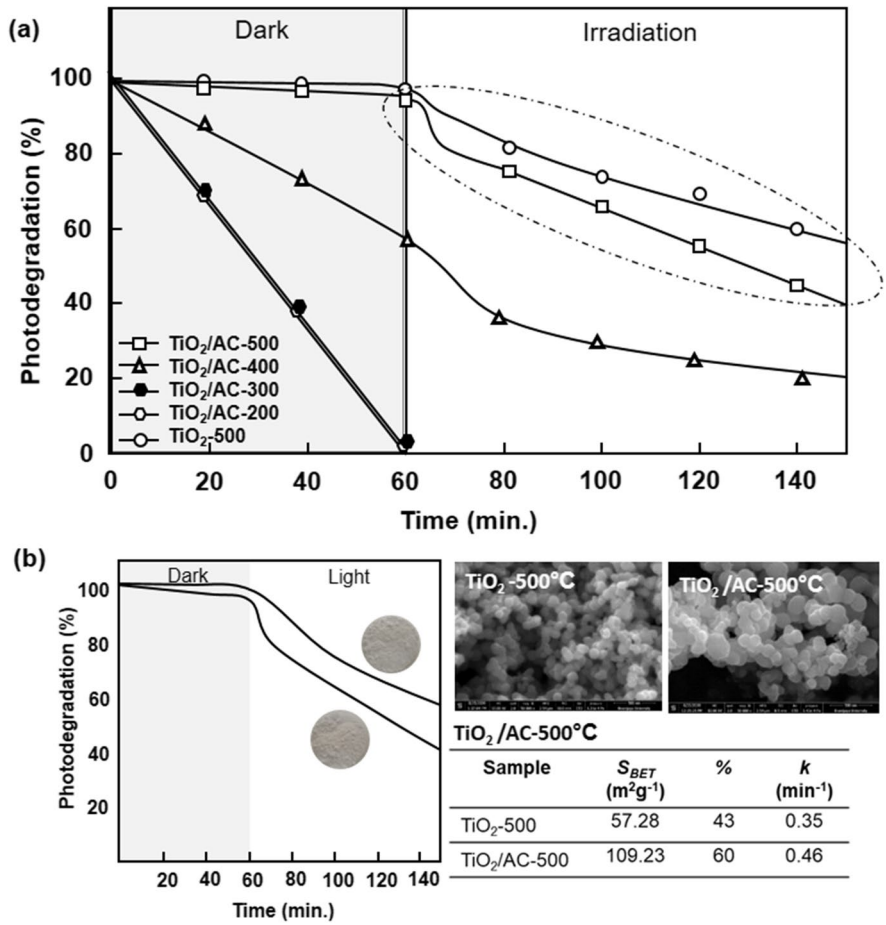

Fig. 8 Photocatalytic degradation of MO under UV-light irradiation (a) over the prepared composite of TiO_2/AC and (b) photocatalytic comparison between TiO_2-500 and TiO_2/AC-500

contributed to the more extensive adsorption activity, as exhibited by TiO_2/AC-200 and 300. Moreover, the zeta potential value of AC is lower than that of MO. Therefore, it allowed for easier absorption of MO on the AC surfaces.

Because of the high adsorption in the sample with high AC content, photocatalytic activity was difficult to observe at low MO ppm. As a result, the role of AC on the degradation of MO over TiO_2/AC-200 and TiO_2/AC-300 was pure as the adsorber. Meanwhile, TiO_2/AC-400 left 60% of MO under dark conditions. In this case, two phenomena (adsorption–photocatalysis) simultaneously occurred, resulting in 80% degradation of MO. In addition, an interesting phenomenon was found. The photocatalytic activity of TiO_2/AC-500 was 20% higher than that of TiO_2-500, although the adsorption ability under the dark condition of both materials was almost similar, implying that the photocatalysis process dominantly caused the degradation of MO.

In order to investigate the transfer efficiency of photogenerated electrons of the AC-TiO_2, specific comparison performance between pure TiO_2-500 and TiO_2/AC-500 is proposed in Fig. 8b. Based on XRD analysis results in Fig. 1, TiO_2-500 had a higher *Dc*, which should have a higher photocatalytic activity than TiO_2/AC-500 (Arutanti et al., 2014b). As discussed earlier, a small amount of AC may be retained within the structure of TiO_2/AC-500 because the specific surface area of TiO_2/AC-500 was two times larger than TiO_2-500. However, the specific surface area did not significantly affect the adsorption process (under dark conditions). Instead, the 1% amount of AC enhanced the photocatalytic activity by providing a large surface area for the reaction site and a large number of vacancies on the surface (Syed et al.,

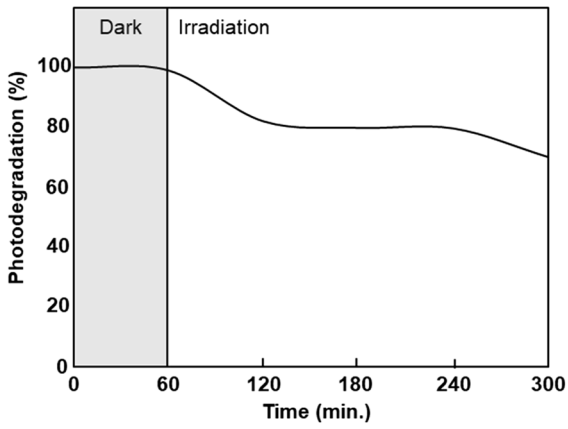

Fig. 9 Photocatalytic degradation of 30 ppm MO under UV-light irradiation over the prepared composite of TiO_2/AC-400

2019). Here, the role of AC on the degradation of MO over TiO_2/AC-500 pure was as an electron trap.

Photodegradation of MO at high concentration is proposed in Fig. 9. Photocatalyst TiO_2/AC-400 was used to decompose 30 ppm of MO under UV irradiation for 4 h. Different from low MO concentration, under high concentration, the MO almost could not be adsorbed by photocatalyst TiO_2/Ac-400 under dark conditions for 1 h. Otherwise, the photocatalytic activity was much better compared to photodegradation of low MO concentration. At high MO concentration, it is clear that the presence of AC significantly affects photocatalyst activity (Fig. 10).

The detailed mechanism of MO photodegradation is explained as follows. In the sample with low AC content (TiO_2/AC-400 and TiO_2/AC-500), AC was trapped into secondary particles almost similar to the core–shell structure, with AC being in the core

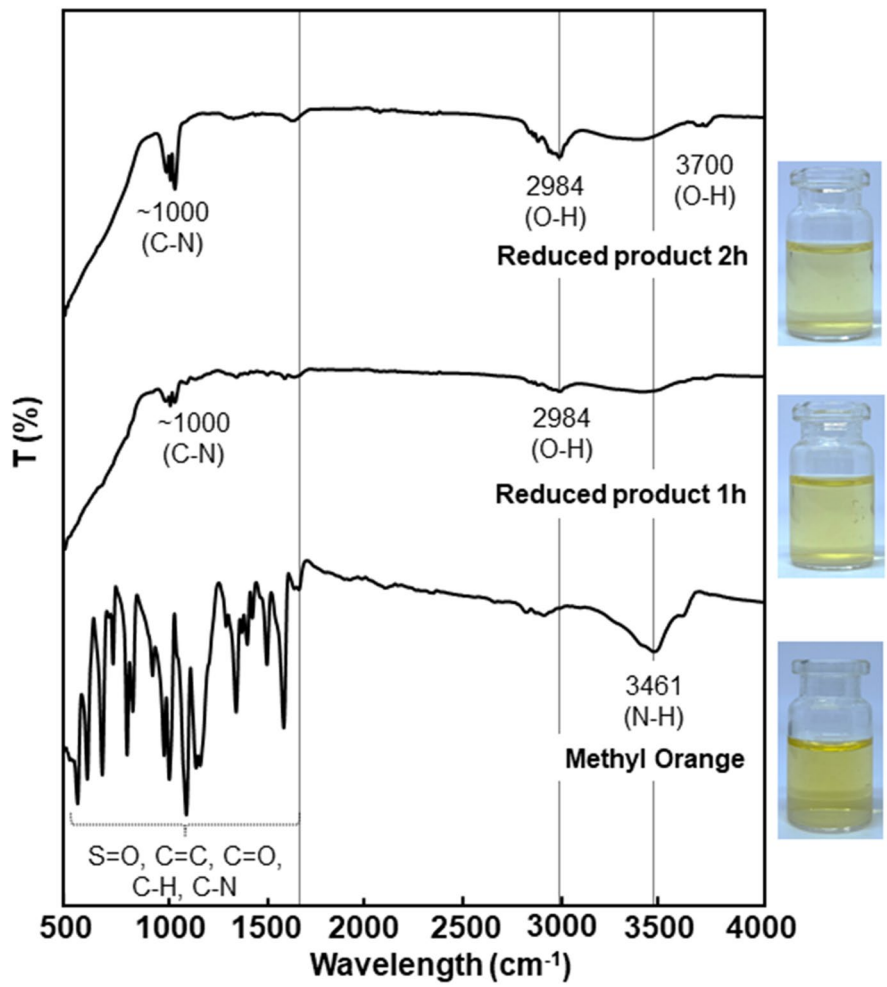

Fig. 10 FTIR spectrum of MO and reduced product MO after 1 and 2 h photocatalytic

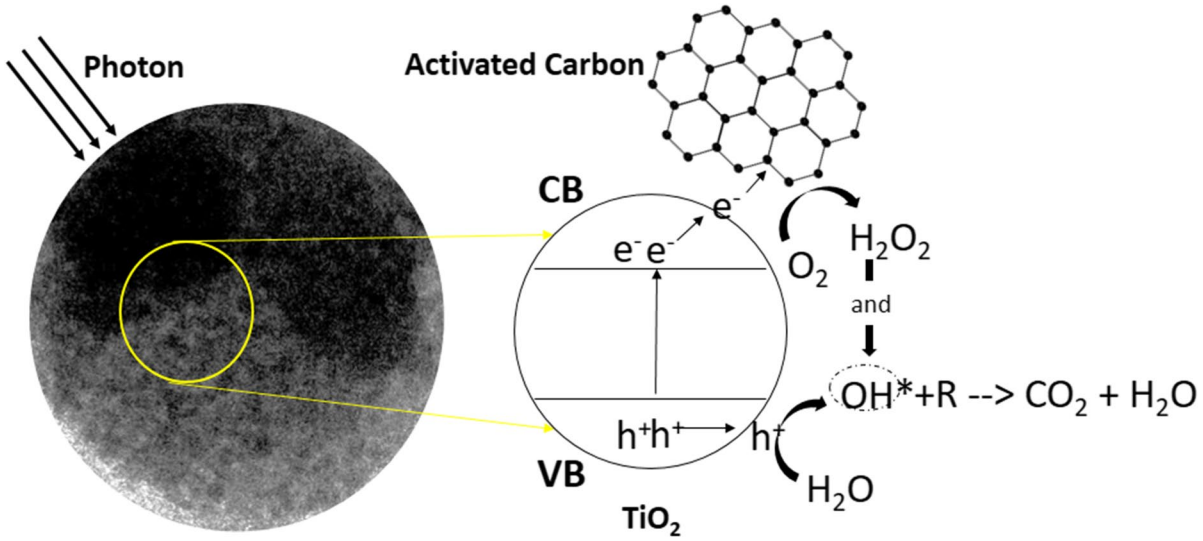

Fig. 11 Photo-adsorption of MO mechanism over the photocatalyst TiO_2/AC under UV-light irradiation

(Fig. 11). During UV-light irradiation, the electrons from the valence band (VB) of TiO_2 excited into the conduction band (CB) generated the pairs of electrons and holes. Holes on the VB reacted with H_2O produced the hydroxyl radical (OH*), while electrons on the CB transferred to the AC surface. Here, the presence of AC as the electron trap to avoid the recombination electron–hole caused the deficiency of photocatalytic activity. Therefore, the electron from AC reacted with O_2 to produce the final products such as anion oxide (O_2^-), H_2O_2, and OH*. Since the OH* has the highest potential energy at 2.8 eV than the organic compounds, hydroxyl radicals could break organic pollutants into carbon dioxide and water molecules (Arutanti et al., 2015). FTIR also studied the photodegradation of methyl orange (Fig. 10) to support the phenomenon. The analysis study focused on the degradation of 4 ppm MO before and after 1 and 2 h of UV irradiation over the TiO_2/AC-400. Some functional groups were observed to decrease. Because of the intense stretching, peaks of S=O, C=C, C=O, C-N, and C-H were found below than wavenumber 1700 cm^{-1} of MO spectrum. Wavenumber 2461 cm^{-1} referred to the presence of N–H stretching. This analysis result is according to the chemical formula of MO $C_{14}H_{14}N_3NaO_3S$ (Chowdhury et al., 2019). The peaks of MO almost disappeared in the spectrum of the photodegraded MO (reduced product) after 1 and 2 h. In the spectra of reduced MO, the peaks at 2984 cm-1 (O–H. water molecule) were found. The stretching (O–H) molecule increased when the MO was degraded after 2 h. The wavelength peak confirmed it at 3700 cm^{-1}. The presence of radical hydroxyl triggered the fragmentation and destruction of the MO group to produce H_zO and CO_2. However, the photodegradation of MO for 2 h was not sufficient to completely reduce C–N stretch, confirmed at 1000 cm^{-1}. The result was also supported by the photograph images, where the MO solution after 2 h photodegraded still has a yellowish color.

This phenomenon proved that, besides providing a high specific surface area to adsorb the organic pollutant efficiently, AC served as an electron trap to avoid the electron–hole recombination resulted in the enhancement of photocatalytic activity.

4 Conclusions

The sol–gel method successfully prepared the composite of TiO_2/AC. However, the post-annealing treatment influenced the characteristics of the prepared photocatalyst. Due to the high specific surface area, four ppm of MO could be 100% adsorbed by TiO_2/AC-200 and TiO_2/AC-300. Annealing temperature at 400 °C was optimum to show the balance phenomena of adsorption–photocatalysis MO. The nanocomposite annealed at this temperature could decompose

almost 80% of MO. This study showed that a small amount of AC in TiO_2/AC nanocomposite effectively served as adsorbent and the electron trap to improve the photocatalytic activity.

Acknowledgements This characterization process was financially supported by ELSA BRIN—National Research and Innovation Agency.

Data Availability All data generated or analyzed during this study are included in this published article [and its supplementary information files].

Declarations

Conflict of Interest The authors declare that they have no conflict of interest.

References

Andriantsiferana, C., Mohamed, E. F., & Delmas, H. (2015). Sequential adsorption - Photocatalytic oxidation process for wastewater treatment using a composite material TiO_2/activated carbon. *Environmental Engineering Research, 20*(2), 181–189. https://doi.org/10.4491/eer.2014.070

Anthonysamy, S. B. I., Afandi, S. B., Khavarian, M., & Mohamed, AR Bin. (2018). A review of carbon-based and non-carbon-based catalyst supports for the selective catalytic reduction of nitric oxide. *Beilstein Journal of Nanotechnology, 9*(1), 740–761. https://doi.org/10.3762/bjnano.9.68

Arutanti, O., Nandiyanto, A. B. D., Ogi, T., Iskandar, F., Kim, T. O., & Okuyama, K. (2014a). Synthesis of composite WO_3/TiO_2 nanoparticles by flame-assisted spray pyrolysis and their photocatalytic activity. *Journal of Alloys and Compounds*. https://doi.org/10.1016/j.jallcom.2013.12.218

Arutanti, O., Nandiyanto, A. B. D., Ogi, T., Kim, T. O., & Okuyama, K. (2015). Influences of porous structurization and pt addition on the improvement of photocatalytic performance of WO_3 particles. *ACS Applied Materials and Interfaces*. https://doi.org/10.1021/am507935j

Arutanti, O., Ogi, T., Nandiyanto, A. B. D., Iskandar, F., & Okuyama, K. (2014b). Controllable crystallite and particle sizes of WO_3 particles prepared by a spray-pyrolysis method and their photocatalytic activity. *AIChE Journal*. https://doi.org/10.1002/aic.14233

Arutanti, O., Sari, A. A., Berkah, A., Nurdin, M., Fitriady, M. A., Parmawati, Y., Rinaldi, N., Yuniarto, A., & Hadibarata, T. (2020). Advanced Degradation of Lignin from Palm Oil Mill Effluent (POME) by a Combination of Photocatalytic-Fenton Treatment and TiO2 Nanoparticle as the Catalyst. Water, Air, and Soil Pollution, 231(6). https://doi.org/10.1007/s11270-020-04617-8

Benkhaya, S., M' rabet, S., & El Harfi, A. (2020). A review on classifications, recent synthesis and applications of textile dyes. In Inorganic Chemistry Communications (Vol. 115). https://doi.org/10.1016/j.inoche.2020.107891

Chowdhury, M., Kapinga, S., Cummings, F., & Fester, V. (2019). Co_3O_4/TiO_2 hetero-structure for methyl orange dye degradation. Water Science and Technology, 79(5). https://doi.org/10.2166/wst.2018.383

Daghrir, R., Drogui, P., & Robert, D. (2013). Modified TiO_2 for environmental photocatalytic applications: A review. In Industrial and Engineering Chemistry Research (Vol. 52, Issue 10, pp. 3581–3599). https://doi.org/10.1021/ie303468t

Esposito, S. (2019). "Traditional" sol-gel chemistry as a powerful tool for the preparation of supported metal and metal oxide catalysts. In Materials (Vol. 12, Issue 4). https://doi.org/10.3390/ma12040668

Hahn, H. H., Logas, J. L., & Averback, R. S. (1990). Sintering characteristics of nanocrystalline tio2. *Journal of Materials Research, 5*(3), 609–614. https://doi.org/10.1557/JMR.1990.0609

Ho, S. J., Yeh, C. W., Kumar, R. V., & Chen, H. S. (2017). Self-organized sol-gel TiO_2 structures: Particles, rectangle tubes, and flower-like slabs. *Materials and Design, 115*, 332–338. https://doi.org/10.1016/j.matdes.2016.11.033

Horikoshi, S., Sakamoto, S., & Serpone, N. (2013). Formation and efficacy of TiO_2/AC composites prepared under microwave irradiation in the photoinduced transformation of the 2-propanol VOC pollutant in air. *Applied Catalysis b: Environmental, 140–141*, 646–651. https://doi.org/10.1016/j.apcatb.2013.04.060

Kartikowati, C. W., Wulansari, A. L., Poerwadi, B., Supriyono, Arif, A. F., Sulistyaningsih, T., & Arutanti, O. (2021). TiO_2 /AC Composites for Adsorption-Photocatalytic of Methyl Orange . IOP Conference Series: Materials Science and Engineering, 1143(1). https://doi.org/10.1088/1757-899x/1143/1/012077

Kibasomba, P. M., Dhlamini, S., Maaza, M., Liu, C. P., Rashad, M. M., Rayan, D. A., & Mwakikunga, B. W. (2018). Strain and grain size of TiO_2 nanoparticles from TEM, Raman spectroscopy and XRD: The revisiting of the Williamson-Hall plot method. *Results in Physics, 9*, 628–635. https://doi.org/10.1016/j.rinp.2018.03.008

Krýsa, J., Baudys, M., Vislocka, X., & Neumann-Spallart, M. (2020). Composite photocatalysts based on TiO_2 – carbon for air pollutant removal: Aspects of adsorption. *Catalysis Today*. https://doi.org/10.1016/j.cattod.2018.09.027

Lee, J. Y., & Jo, W. K. (2012). Control of methyl tertiary-butyl ether via carbon-doped photocatalysts under visible-light irradiation. *Environmental Engineering Research, 17*(4), 179–184. https://doi.org/10.4491/eer.2012.17.4.179

Lellis, B., Fávaro-Polonio, C. Z., Pamphile, J. A., & Polonio, J. C. (2019). Effects of textile dyes on health and the environment and bioremediation potential of living organisms. Biotechnology Research and Innovation, 3(2). https://doi.org/10.1016/j.biori.2019.09.001

Lim, T. T., Yap, P. S., Srinivasan, M., & Fane, A. G. (2011). TiO_2/AC composites for synergistic adsorption-photocatalysis processes: Present challenges and further developments for water treatment and reclamation. *Critical Reviews in Environmental Science and Technology, 41*(13), 1173–1230. https://doi.org/10.1080/10643380903488664

Lu, L., Shan, R., Shi, Y., Wang, S., & Yuan, H. (2019). A novel TiO_2/biochar composite catalysts for photocatalytic degradation of methyl orange. *Chemosphere*. https://doi.org/10.1016/j.chemosphere.2019.01.132

Ouzzine, M., Romero-Anaya, A. J., Lillo-Ródenas, M. A., & Linares-Solano, A. (2014). Spherical activated carbon as an enhanced support for TiO_2/AC photocatalysts. *Carbon, 67*, 104–118. https://doi.org/10.1016/j.carbon.2013.09.069

Parashar, M., Shukla, V. K., & Singh, R. (2020). Metal oxides nanoparticles via sol–gel method: a review on synthesis, characterization and applications. In Journal of Materials Science: Materials in Electronics (Vol. 31, Issue 5, pp. 3729–3749). https://doi.org/10.1007/s10854-020-02994-8

Peñas-Garzón, M., Gómez-Avilés, A., Bedia, J., Rodriguez, J. J., & Belver, C. (2019). Effect of activating agent on the properties of TiO_2 /activated carbon heterostructures for solar photocatalytic degradation of acetaminophen. *Materials*. https://doi.org/10.3390/ma12030378

Qi, K., Cheng, B., Yu, J., & Ho, W. (2017). A review on TiO_2-based Z-scheme photocatalysts. In Cuihua Xuebao/Chinese Journal of Catalysis (Vol. 38, Issue 12, pp. 1936–1955). https://doi.org/10.1016/S1872-2067(17)62962-0

Soleymani Naeini, M., Ghorbani, M., & Chambari, E. (2019). Synthesis of Composite Coating Containing TiO_2 and HA Nanoparticles on Titanium Substrate by AC Plasma Electrolytic Oxidation. *Metallurgical and Materials Transactions a: Physical Metallurgy and Materials Science, 50*(7), 3310–3319. https://doi.org/10.1007/s11661-019-05251-8

Subramani, A. K., Byrappa, K., Kumaraswamy, G. N., Ravikumar, H. B., Ranganathaiah, C., Lokanatha Rai, K. M., Ananda, S., & Yoshimura, M. (2007). Hydrothermal preparation and characterization of TiO_2:AC composites. *Materials Letters, 61*(26), 4828–4831. https://doi.org/10.1016/j.matlet.2007.03.050

Syed, N., Huang, J., Feng, Y., Wang, X., & Cao, L. (2019). Carbon-Based Nanomaterials via Heterojunction Serving as Photocatalyst. In Frontiers in Chemistry (Vol. 7). https://doi.org/10.3389/fchem.2019.00713

Yin, Y., Ruan, D., & Hou, F. (2017). Synthesis of heterostructure Cu_2O/TiO_2 nanotube arrays by AC electrochemical deposition. *Ferroelectrics, 521*(1), 94–100. https://doi.org/10.1080/00150193.2017.1390968

Zhang, X., & Lei, L. (2008). Effect of preparation methods on the structure and catalytic performance of TiO_2/AC photocatalysts. *Journal of Hazardous Materials, 153*(1–2), 827–833. https://doi.org/10.1016/j.jhazmat.2007.09.052